Structural Control for a Circular Plate

J.-N. Aubrun* and M.J. Ratner†
Lockheed Palo Alto Research Laboratory, Palo Alto, California
and
M.G. Lyons‡
Integrated Systems, Inc., Palo Alto, California

This paper describes the detailed approaches and experimental results for controlling both the rigid body and structural modes of a 1.2-m-diam circular plate. The experiments demonstrate required methodology and expected pathologies in effecting modal control with both colocated and noncolocated actuators and sensors. Optical sensing, along with electromagnetic and electrodynamic actuators, is used to control five structural bending modes.

Introduction

ALTHOUGH the experimental body of knowledge in large space structures (LSS) control has grown much more slowly than the selection of theoretical control approaches over the past five years, several important experiments have been performed, especially under the auspices of the DARPA/Active Control of Space Structures (ACOSS) Program. Many of these experiments are described in Vol. III of Ref. 1 by Strunce et al., the descriptive list is reproduced in Table 1. Although additional researchers are now engaged in developing LSS control experiments, the ones shown in the table represent the first major attempts to study LSS control strategies in the laboratory. Reference 1 also provides an excellent bibliography and overview of current LSS control technologies. The purpose of this paper is to describe the approaches and to present some detailed results from the Lockheed circular plate experiment.

This experiment attempted to combine many of the features and requirements of LSS control problems, namely: 1) low natural damping and closely distributed modal frequencies, 2) colocated and noncolocated modal conrol, 3) real time digital mechanization, and 4) optical figure sensing methods. Because of this combination of requirements and methodologies, the test objectives and procedures were complex and demanding. In some cases, maximum likelihood system identification techniques, for example, were required for data analysis. This paper will focus principally on the objectives and results of this experiment with only an indication of the pathological problems encountered.

The experiment was constructed to examine problems in LSS hardware mechanization as opposed to evaluating various control synthesis theories. Both colocated rate feedback (low-authority, LAC[1]) and noncolocated state estimator (high-authority, HAC[1]) kinds of mechanizations were studied in both analog and digital forms. A variety of techniques could be used to synthesize these controllers. These details are left as material for a separate paper.[2]

Experiment Description

The circular plate (CP) experiment had three main objectives. First, the validation of the HAC/LAC approach on a highly resonant structure with nearly repeated modal frequencies, with a control system including both attitude and vibration control; second, the demonstration of the use of two new pieces of hardware: the Pivoted Proof Mass actuator (PPM) and the microphase optical sensor (μ-phase sensor), which were both included for the first time in an optimal control scheme; third and finally, the demonstration of high-speed digital mechanizations (125-Hz sampling rate) and the use of almost the full Nyquist range by the controller. A photograph of the experimental setup is shown in Fig. 1.

The structure to be controlled is a flat aluminum circular plate, 1.2 m diameter and about 3 mm (1/8 in.) thick. It is suspended vertically by a system of springs and strings attached near its center as shown in Fig. 2. This device provides nearly unrestrained boundary conditions for the plate, with the first three rigid body modes (x and y rotation, z translation) around or below 0.3 Hz, while the first bending mode occurs at about 19 Hz. The suspension system is attached to a frame mounted on a 14-ft-long optics table to provide further insulation from ground vibrations. (The whole table actually can be floated on air bags. This feature was not exercised, however.) The frame and the plate are enclosed in a soundproof cabinet, with a plexiglass window in its front, to further reduce disturbances due to acoustic vibrations and air currents.

Sensors and Actuators

The sensing system is purely optical. Although two accelerometers were used in preliminary tests, they were abandoned because of adverse characteristics.

Instead, four corner-cube mirrors were mounted on the plate and were used in conjunction with the μ-phase sensor which measured their position along the z axis by comparing the phase between outgoing and reflected laser beams. Also, two flat mirrors on the top reflected laser beams which were sensed by two two-dimensional linear photodetectors (Fig. 3). Each detector measures the rotations about the y' and x' axes of the plate (x'/y' axes are rotated by +45 deg from the x/y axes).

Actuation is provided by three contactless actuators, for attitude and vibration control, and two PPM actuators, for vibration control or disturbance injection. These actuators were described in detail in the ACOSS 5 final report.[3]

In Fig. 4 a recapitulation of the actuator/sensor system is shown with a nomenclature and numbering which will be used throughout this report. Table 2 shows the participation of these actuators and sensors in both the control system and evaluation procedure. Six sensors and four actuators were used for control purposes. The remaining actuator (PPM) was used to excite the specimen with various disturbances. The last

Submitted Aug. 23, 1983; revision received Feb. 1, 1984.

*Senior Staff Scientist, Guidance and Control Laboratory.
†Staff Scientist, Guidance and Control Laboratory.
‡Vice President.

Table 1 Relevant LSS experiments

Company	Type	Description	Sensor	Actuator	Demonstration
Draper	Beam	Fixed-free ¼ × 1 × 60 in. aluminum	Piezoelectric accelerometers	Electrodynamic shaker	Observation/control spillover modern modal control
	Beam	Fixed-free 40 in. magnesium	Optical rate sensor	Proof-mass	Low-authority control
	I-Beam	Fixed-free 26 × 16 in. (400 lb) aluminum	Optical rate sensor	Single gimbal CMG	Low-authority control
	Vertical beam	Fixed-free 6 in. aluminum lead tip masses	Accelerometers, quad-detector photodiodes	Pivoted proof-mass	Low-authority control system identification
Lockheed	Circular plate	Suspended 2 m-diam aluminum	Multichannel microphase optics	Pivoted proof-mass	Low-authority control Low/high-authority control system identification
	POC	Suspended 4.5 m boom, 3 m reflector, aluminum	Accelerometers, rate gyros, laser	CMG, proof-mass	Classical and modern control of vibration and slew
	TOYSAT	Suspended rigid body 1.6 m cantilever beams aluminum	Accelerometers, LVDT velocity pickoffs	Electrosesis actuators	Open-loop torque profile high-authority control
Convair	Plate	Fixed-free 68 × 103 in. aluminum 4 × 5/16 in. welded beams	Rate gyros	Torque wheels	Model error sensitivity suppression
JPL	Beam	Pinned-free 150 × 6 × 1/32 in. stainless steel	Eddy current position sensor	Brushless dc torque motor	Modern modal control
LaRC	Beam	12 × 6 × 3/16 in. aluminum	Noncontacting deflection sensor, load sensor	Electrodynamic shaker	–
TRW	Plate	Clamped 1.73 m × 1.22 m × 1.66 mm aluminum	Rate sensors, accelerometers	Bending moment actuator	Vibration suppression and damping augmentation

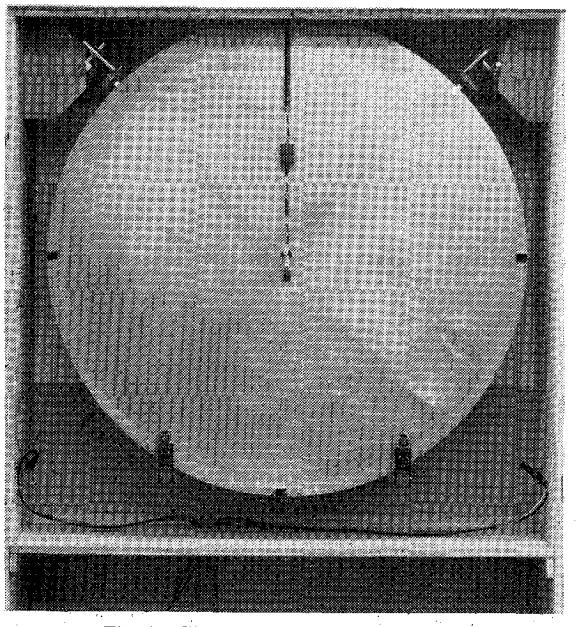

Fig. 1 Circular plate experiment setup.

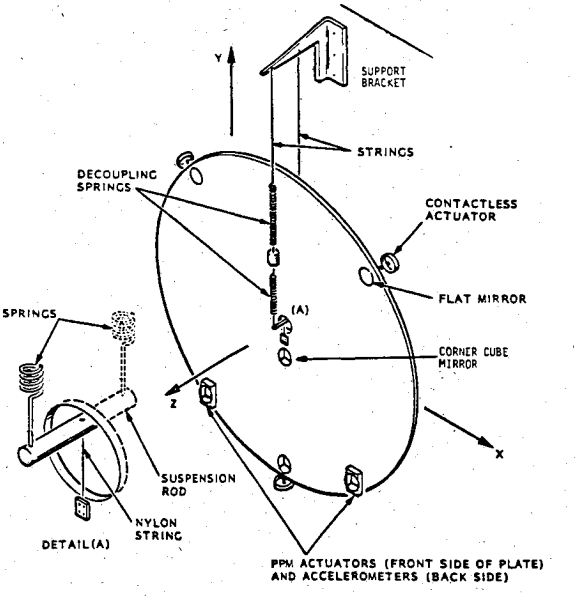

Fig. 2 Experiment general schematic.

two optical sensors provided supplementary information for evaluation purposes and an independent check of the system.

Control Synthesis Model

From the SPAR finite element model obtained earlier, system matrices were generated corresponding to the state equations

$$\dot{x}=Fx+Gu, \qquad y=Hx \tag{1}$$

(The state vector x is described in Table 2, along with the vectors u and y.)

The natural vibration modes of the plate are shown in Fig. 5. Note that for certain modes, some actuators or some sensors are situated on a nodal line, making them uncoupled from these particular modes.

The goal of the experiment was the control of the modes shown on the top line, as the sampling rate limitation to 125 Hz made it impossible to control the higher modes. Three more degrees of freedom of the plate had to be controlled also, the two rotations and the translation along the z axis. Thus, a total of $3+5=8$ degrees of freedom was used, making up a 16-state control synthesis model. This model, rewritten in discrete form, is given by:

Table 2 Control, measurement, and state vector definition

Control vector	Actuator no.	Type	Action	Comments
u_1	1	PPM	z force	Control inputs
u_2	2	CEM	z force	provided by the
u_3	3	CEM	z force	controller
u_4	4	CEM	z force	
u_5	5	PPM	z force	Used for excitation only
Measurement vector	**Sensor no.**	**Type**	**Sensed quantity**	
y_1	1	μ phase	z motion	Sensor inputs to
y_2	2	μ phase	z motion	the controller
y_3	3	angular	x' rotation	
y_4	4	angular	y' rotation	
y_5	5	angular	x' rotation	
y_6	6	angular	y' rotation	
y_7	7	μ phase	z motion	Used for characterization
y_8	8	μ phase	z motion	only
State vector	**Variable**	**Definition**		
x_1	$\dot{\theta}_x$	x rotation		Rigid body modes
x_2	θ_x	x rotation		
x_3	$\dot{\theta}_y$	y rotation rate		
x_4	θ_y	y rotation		
x_5	$\dot{z}$	z-translation velocity		
x_6	z	z-translation		
x_7	$\dot{q}_1$	1st rate		Bending mode amplitudes and rates
x_8	q_1		amplitude	
x_9	$\dot{q}_2$	2nd rate		
x_{10}	q_2		amplitude	
x_{11}	$\dot{q}_3$	3rd rate		
x_{12}	q_3		amplitude	
x_{13}	$\dot{q}_4$	4th rate		
x_{14}	q_4		amplitude	
x_{15}	$\dot{q}_5$	5th rate		
x_{16}	q_5		amplitude	

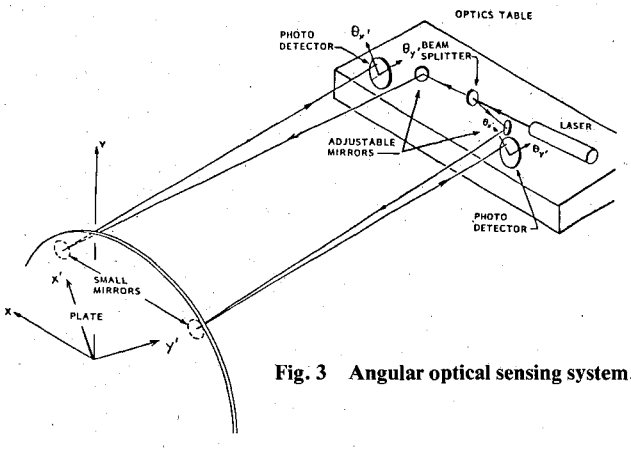

Fig. 3 Angular optical sensing system.

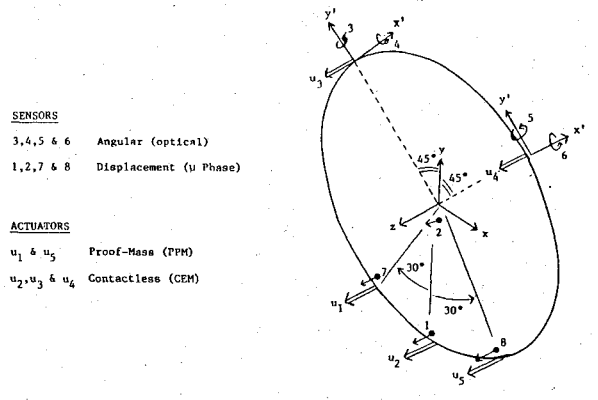

Fig. 4 Sensors and actuators definition.

$$x_{n+1} = \phi x_n + \Gamma u_n, \qquad y_n = H x_n \tag{2}$$

Thus, the state observer equations are

$$\hat{x}_{n+1} = \phi \hat{x}_n + \Gamma u_n + k(y_n - H\hat{x}_n) \tag{3}$$

and the control laws take the form

$$u_n = C\hat{x}_n \tag{4}$$

The control synthesis process consists of finding the values of K and C, the filter and control gain matrices, respectively. Then Eqs. (3) and (4) can be implemented in a microprocessor (in this case, the CPSI map 300 Array Processor). The array processor (AP) receives the vector of measurements, y_n, as an input, and delivers the vector of actuation commands, u_{n+1}, according to an internal algorithm described by the matrix-vector multiplication:

$$\begin{bmatrix} \hat{x}_{n+1} \\ u_{n+1} \end{bmatrix} = A \begin{bmatrix} \hat{x}_n \\ u_n \\ y_n \end{bmatrix} \tag{5}$$

Table 3 Circular plate test matrix control experiments

	Test #	Purpose	Controller type	Actuators, no. and type	Modes controlled	Disturbance types	Remarks
	1	System and calibrations checkout	Classical (PID)	2 CEM	2 Rigid	1, 2	Digital implementation of analog stabilizer; 2 optical sensors only. Total of 4 states.
	2	Filter algorithm and accelerometers checkout	HAC	2 CEM	3 Rigid	1, 2	4 Optical sensors and 2 accelerometers
	3	Effects of LAC	HAC + LAC				Total of 6 states
	4	Demonstration of modal control	HAC + LAC	2 CEM	3 Rigid 2 Bending	1, 2	
Not performed	5	Demonstration of steady-state disturbance rejection Effects of disturbance variation	HAC + LAC	2 CEM 2 PPM 1 CEM excciter	3 Rigid 2 Bending	1, 2, 3	Total of 15 states
	6	Multimode control	HAC + LAC	2 CEM 2 PPM	3 Rigid 5 Bending	1, 2	Total of 19 states
	7	Microphase optics checkout	HAC/LAC	3 CEM	3 Rigid	1, 2	1 μ-phase sensor for translational mode
	8	Microphase optics demonstration for multimode control	HAC/LAC	3 CEM 1 PPM	3 Rigid 5 Flexible	1, 2	16 States 6 Sensors

Note: Disturbances: 1) environmental noise, 2) step function, 3) sinusoidal.

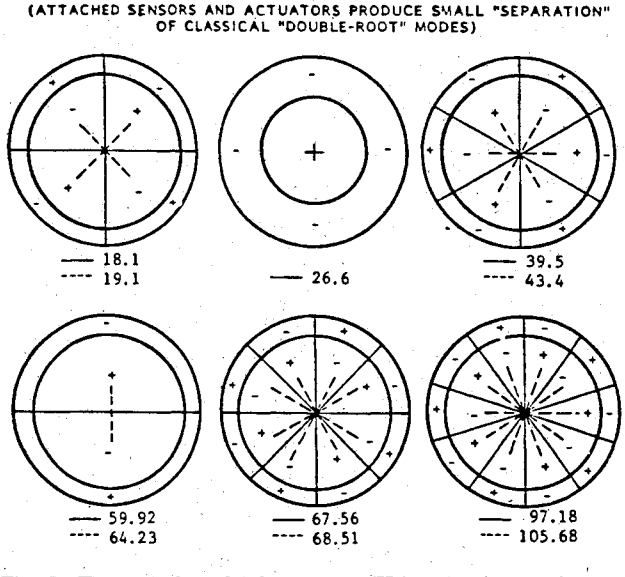

Fig. 5 Theoretical modal frequencies (Hz) and patterns of the circular plate.

where

$$A=\begin{bmatrix} \phi-KH & \Gamma & K \\ C(\phi-KH) & C\Gamma & CK \end{bmatrix}$$

It is easily shown that matrix (5) is equivalent to Eqs. (3) and (4); however, this formulation is a more efficient way for programming the AP.

Because of the importance of determining the behavior of the state estimator, it is required that the time histories of the full input vector $[x_n, u_n, y_n]^T$ be examined. This program, however, slows down the algorithm considerably and thus sampling rates were limited to 125 Hz.

The general configuration of the system is shown in Fig. 6, in which the links between the different processors are shown.

Table 4 Results of the first series of tests

Experimental difficulties	Corrective step taken
Poor rigid body controllability with the 2 top CEM only	Use of a third CEM at bottom of plate
Bad characteristic of accelerometer at low frequency → rigid body problems	Replacement of accelerometers by μ-phase displacement sensors
Unverified plate model	Identification of critical elements
Filter evaluation	Use of static observer. Add two more sensors for cross-check.

Because of the independence of the AP relative to the host processor, the latter can be used to characterize the system independently during closed-loop operations without affecting the control algorithm.

Test Plan

The test plan originally established included control based on the use of two accelerometers. However, due to inherent difficulties that revealed themselves during the tests, some of these tests had to be cancelled and, instead, more tests were performed with the μ-phase sensor, which turned out to be a very reliable and precise sensor. Table 3 shows a matrix overview of the test plan and the modifications that were made during the course of the study. As can be seen, tests 5 and 6 were dropped, to the benefit of tests 7 and 8 which have been successfully accomplished. The chart shows the different types of controllers to be tested and the objectives of each of them. The actuators in use in each case are listed as contactless electromagnetic (CEM) or pivoted proof-mass (PPM).

Tests 1 to 4 were discussed in Ref. 4 and, except for the significant conclusions, will not be detailed here.

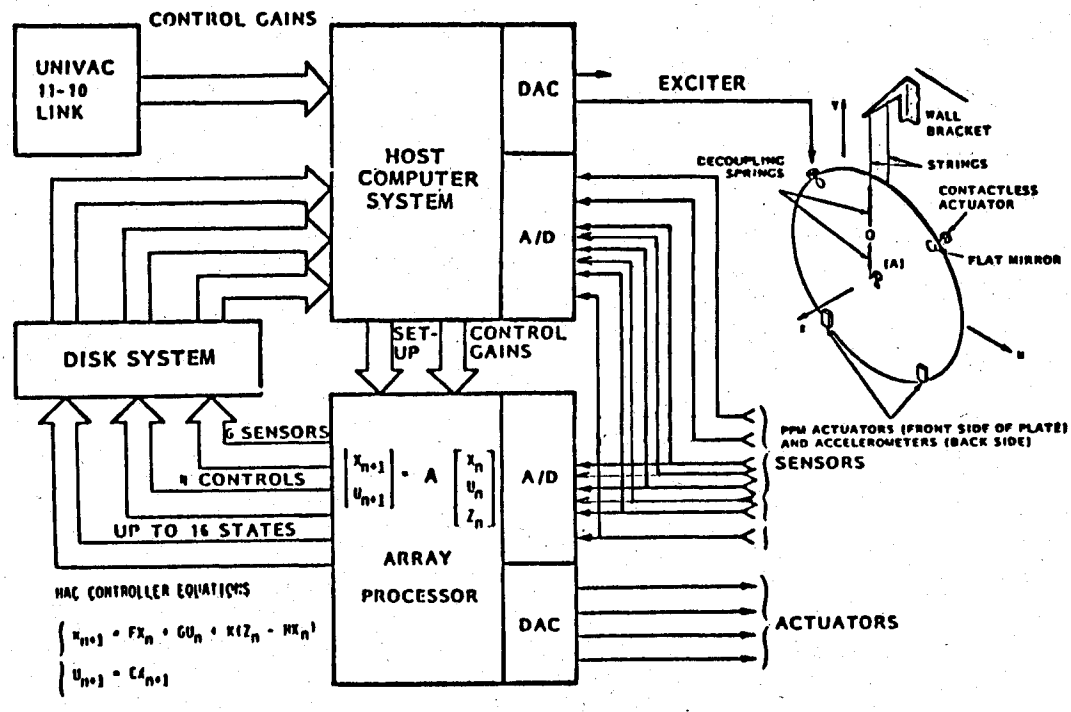

Fig. 6 Experiment overall configuration.

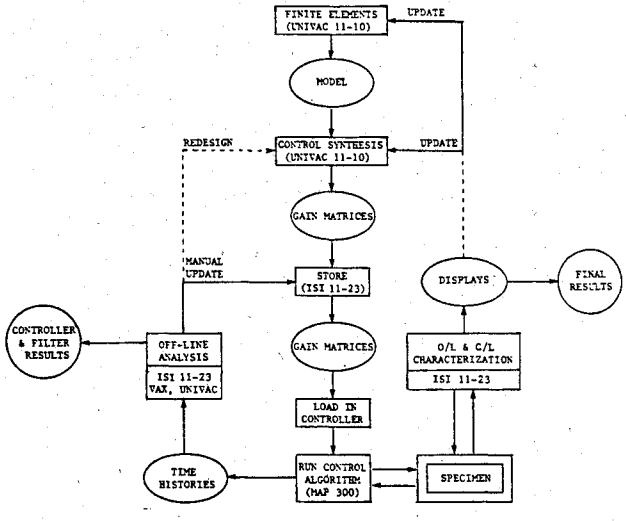

Fig. 7 Structural control experiment procedure.

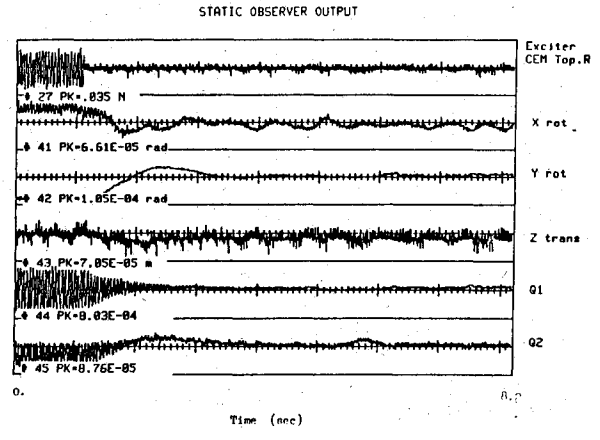

Fig. 8 Response to excitation at first bending mode frequency.

Test 8 constitutes the main achievement of this study, since it includes all the features of the ACOSS methodology and will be discussed in the following section. Within the modifications made necessary by the experimental findings, the test plan has been followed and executed successfully. The actual experimental results are discussed next.

Experimental Results

Preliminary Tests

Preliminary open-loop tests were performed on the plate to determine the frequencies and damping ratios of the first five bending modes. The various resonances were found directly by a search-and-dwell procedure. The plate was excited with sinusoidal signals of adjustable frequency driving a CEM actuator until maximum sensor response. The free decay was measured to determine the damping ratio. This method was the easiest and most accurate because the damping ratios were very small, about 0.0003 for modes 1 and 2, 0.0013 for mode 3, and 0.0004 for modes 4 and 5.

These results showed that the suspension system and the aerodynamic effects were not introducing significant amounts of damping in the structure. The measured damping ratios were even lower than those generally expected in Large Space Structures (<0.005), making the control problem at least as difficult.

Control Experiment Procedure

The various operations involved in the structural control experiments are shown in Fig. 7. From the finite element analysis, a linear model is derived which is used as a basis for performing directly digital control synthesis. At the AP maximum sampling rate of 125 Hz, the time delay between samples is 8 ms. During this time, the processor must perform the operations described earlier in Eq. (5). Thus, there is an 8-ms delay between the input to the AP (from the sensors) and its output (to the actuators). The additional delays introduced by the dynamics of sensors and actuators themselves are negligible in comparison.

The bandwidth of the optical sensors being greater than 5 kHz has no effect on the control system. The actuators are preceded by anti-aliasing filters with a resulting bandwidth of about 70 Hz, which still does not have a significant impact on

the controller. Therefore, except for the 8-ms delay due to sampling, which was exactly represented, no actuator or sensor dynamics is used in the discrete model.

The control synthesis program generates a set of gain matrices which are stored in the LSI 11-23 and may be manually updated if needed. The appropriate set is loaded into the array processor. The control algorithm is then started and the AP controls the specimen and may acquire data. These data are stored on disk and can be analyzed off-line by the 11-23 or transmitted to a larger computer (VAX or UNIVAC 1110) for further processing. Also, while the AP is running, dynamic characterizations may be carried out by the 11-23.

Implementation of the LAC System

Because of the inner velocity servo loop that is used on the PPM actuators, some active damping is automatically provided without any other external loop. In fact, the actuators' dynamics mimic a passive inertial damper. For this reason, their inner loop damping capability is limited, but is nevertheless sufficient to stabilize most of the HAC control laws. Therefore, as long as the PPM actuators were used in the control scheme, they were automatically introducing a LAC type of stabilization. The only way to study the HAC system by itself is to utilize only the CEM actuators in the control synthesis. In all cases studied, whether attitude control only or full attitude and vibration control was employed, the HAC system alone always showed instabilities due to spillover. These instabilities would disappear as soon as the PPMs were turned on (whether or not they were included in the control scheme).

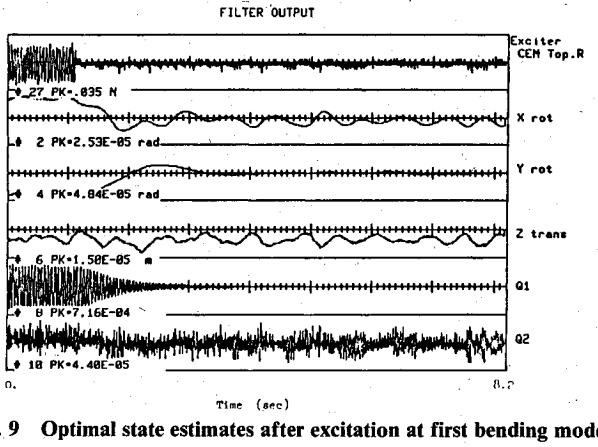

Fig. 9 Optimal state estimates after excitation at first bending mode frequency.

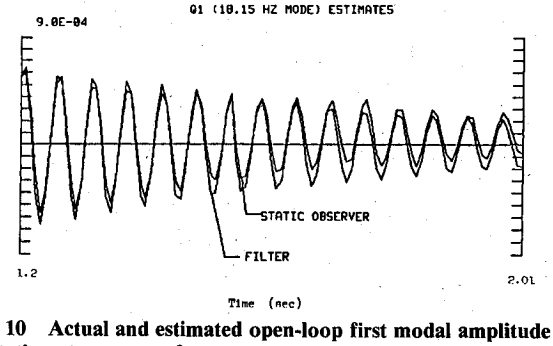

Fig. 10 Actual and estimated open-loop first modal amplitude after excitation at resonance frequency.

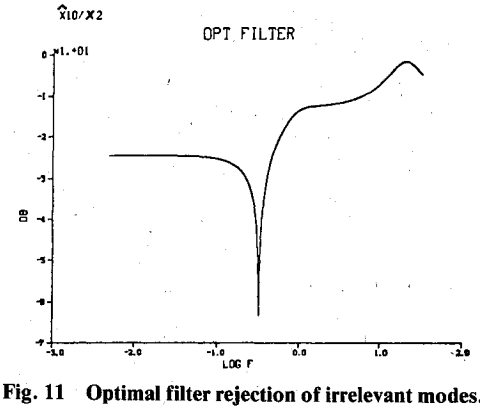

Fig. 11 Optimal filter rejection of irrelevant modes.

Early Experimental Results

The first test that utilized the AP (test 1) was meant to be a check of the correct functioning of the different subsystems, actuators, sensors, and microprocessors, and the calibration factors. A simple classical attitude controller was implemented successfully and controlled the two rotations about the X and Y axes within a few microradians (5 μrad rms).

An optimal controller was then synthesized to control the same two rotations, plus the Z translation, to which the accelerometers were sensitive. Finally, control of the first two bending modes was added to this controller's function. In all these cases, the only actuators being used for HAC were the two top CEM actuators, while, as explained previously, the PPM actuators were providing the LAC stabilization.

These last two tests were only partially successful in that the performance obtained was very low and not in good agreement with predictions. Table 4 summarizes the main difficulties encountered and the steps that were taken to alleviate them and continue the experiments.

Static Observer Implementation

The introduction of the two μ-phase measurements, the bottom and center Z displacements, made possible the construction of a static observer. Indeed, six measurements were available (four local rotations and two local displacements) and thus the two rigid body rotations, the Z translations, and the next three bending modes could be reconstructed from them. If one assumes that no other mode is excited, the following relation is true:

$$y[z_1,z_2,\theta_1,\theta_2,\theta_3,\theta_4] = H_0[\theta_x,\theta_y,z,q_1,q_2,q_3] \qquad (6)$$

where H_0 is a 6×6 matrix. Because of the particular choice of sensors, the matrix is invertible (i.e., the quantities $(\theta_x,\theta_y,\ldots,q_3)$ are statically observable and thus their estimates can be obtained by

$$[\theta_x,\theta_y,z,q_1,q_2,q_3] = H_0^{-1}y \qquad (7)$$

Of course, this estimate is corrupted by sensor calibration errors, sensor noise, and the fact that Eq. (6) is a truncation since the right side should contain all the other modal amplitudes, q_4, q_5, etc. However, the static observer defined by Eq. (7) is still very useful to make a rough check of the Kalman filter.

Filter Study

The critical part of an optimal controller is usually the filter, or state observer; thus it needs to be carefully studied first. An HAC controller was designed after modifications 1 and 2 of Table 4 were implemented. This controller was to control the three rigid body modes plus the first two bending modes, introducing about 5% damping in these modes. The experiment showed severe instabilities, which were removed when no modal control was applied. A semiopen-loop test was thus made to check the behavior of the filter. Figures 8-10 show the main result obtained. In Fig. 8 a static observer

determined these five modal responses to an excitation at the first bending frequency. The top trace shows the excitation; next are the three rigid body and two lowest bending responses. As one would expect, the input excites primarily the first bending mode. Only the rigid body mode could be controlled in this test because feeding back the bending states caused instability.

The output of the filter is shown in Fig. 9. The state estimates of the optimal filter must match the previous statically observed states for the controller to work. X_{rot}, Y_{rot}, and Z_{trans} are the three controlled rigid body state estimates, Q_1 and Q_2 the two uncontrolled bending-state estimates (18.1 and 19.1 Hz). The rigid body estimates match the corresponding states in the preceding figure, indicating correct frequencies and mode shapes for the rigid body modes. The optimal estimate histories show how the filter attenuates the measurement noise in the statically observed states.

Finally, as shown in Fig. 10, the filter seems to estimate the first bending mode correctly when no attempt is made to control the latter. The fact that this mode becomes unstable in closed loop indicates the possibility of errors in the value of the control input matrix G.

Another effect was discovered which appears to be fundamental for this type of controller. Since the optimized filter was suspected of giving wrong answers in closed loop, the static observer was used instead, with the additions of band pass filters to reduce the noise and discriminate between the states. Basically, the pseudostatic observer was defined by

$$\ddot{\tilde{x}}_i + 2\zeta_i\omega_i\dot{\tilde{x}}_i + \omega_i^2\tilde{x}_i = H_{ij}^{-1}y_j \qquad (8)$$

The instability disappeared with this filter, although the performance was still poor. Further tests showed that the instability was caused by the rigid body states being improperly driven by the modal states, due to insufficient rejection of these states by the optimal filter. A comparison of the transfer functions for the optimal filter with the quasistatic observer shows this phenomenon more clearly. The transfer functions compared are from an actual rigid body state (x_2 and Y rotation angle) to the estimate of a modal state (x_{10}, the second bending mode amplitude). In Fig. 11 is shown the response of the optimal filter. This open-loop frequency response explains the sensitivity of controller stability to model error. The bending state estimation puts a notch at a rigid body resonant frequency to eliminate the irrelevant state's contribution to the measurements. This allows low-filter gains that minimize transmission of broadband measurement noise. The rejection of signals at nonresonant frequencies is low, so the system stability is sensitive to errors in the modeled open- or closed-loop resonant frequencies.

By contrast, the response of the quasistatic observer shown in Fig. 12 shows a very significant rejection of irrelevant modes, at all frequencies.

This filter indeed makes use of spatial discrimination much more than the optimal filter does. The drawback of such a filter, however, is its low performance in terms of sensor noise rejection. The optimal filter reduces this noise by relying on the exact knowledge of the modal frequencies, thus its increased sensitivity to errors.

Model Refinement

In order to progress in the experiment, it was decided to proceed to a limited parameter identification to improve the

Table 5 16-State control synthesis model

F Matrix is 16×16	Non-zero elements follow						
1, 1,	9.9971−01,	1, 2,	−3.3148−02,	2, 1,	7.9990−03,	2, 2,	9.9987−01
3, 3,	9.9985−01,	3, 4,	−1.1887−02,	4, 3,	7.9995−03,	4, 4,	9.9995−01
5, 5,	9.9940−01,	5, 6,	−8.5019−02,	6, 5,	7.9980−03,	6, 6,	9.9966−01
7, 7,	5.8806−01,	7, 8,	−8.8732+01,	8, 7,	6.8229−03,	8, 8,	6.1607−01
9, 9,	5.6279−01,	9,10,	−9.7237+01,	10, 9,	6.7728−03,	10,10,	5.7703−01
11,11,	2.2018−01,	11,12,	−1.6107+02,	12,11,	5.7547−03,	12,12,	2.3558−01
13,13,	−4.0377−01,	13,14,	−2.2275+02,	14,13,	3.6166−03,	14,14,	−3.8600−01
15,15,	−5.7308−01,	15,16,	−2.2296+02,	16,15,	2.9984−03,	16,16,	−5.7162−01
G Matrix is 16×4	Non-zero elements follow						
1, 1,	−2.7125−03,	1, 2,	−3.1460−03,	1, 3,	2.3814−03,	1, 4,	2.3814−03
2, 1,	−1.0850−05,	2, 2,	−1.2585−05	2, 3,	9.5259−06,	2, 4,	9.5259−06
3, 1	1.6719−03,	3, 2,	−2.1199−12,	3, 3,	2.3646−03,	3, 4,	−2.3646−03
4, 1,	6.6877−06,	4, 2,	−8.4796−15,	4, 3,	9.4585−06,	4, 4,	−9.4585−06
5, 1,	5.5186−04,	5, 2,	5.5186−04,	5, 3,	5.5186−04,	5, 4,	5.5186−04
6, 1,	2.2077−06,	6, 2,	2.2077−06,	6, 3,	2.2077−06,	6, 4,	2.2077−06
7, 1,	3.6175−03,	7, 3,	−5.8336−03,	7, 4,	5.8336−03,	8, 1,	1.5652−05
8, 3,	−2.5241−05,	8, 4,	2.5241−05,	9, 1,	9.9831−04,	9, 2,	5.7908−03
10, 1,	4.3425−06,	10, 2,	2.5189−05,	11, 1,	2.0924−03,	11, 2,	1.2603−03
11, 3,	1.9681−03,	11, 4,	1.9681−03,	12, 1,	9.9300−06,	12, 2,	5.9810−06
12, 3,	9.3401−06,	12, 4,	9.3401−06,	13, 1,	3.6166−08,	13, 3,	2.5316−03
13, 4,	−2.5316−03,	14, 1,	2.2504−10,	14, 3,	1.5753−05,	14, 4,	−1.5753−05
15, 1,	1.1124−04,	15, 2,	3.0584−03,	15, 3,	1.9430−03,	15, 4,	1.9430−03
16, 1,	7.8412−07,	16, 2,	2.1558−05,	16, 3,	1.3696−05,	16, 4,	1.3696−05
H Matrix is 6×16	Non-zero elements follow						
1, 2,	−5.8635−01,	1, 6,	1.0000+00	1,10,	8.5500−01,	1,12,	2.1900−01
1,16,	1.0200+00,	2, 2,	−3.2908−02,	2, 6,	1.0000+00,	2,10,	−1.1550−01
2,12,	−5.1400−01,	2,16,	−1.4140−02,	3, 2,	−7.0710−01,	3, 4,	7.0710−01
3, 8,	−6.7400−02,	3,10,	−1.9000+00,	3,12,	−2.5600−01,	3,14,	−2.1528+00
3,16,	2.3930+00,	4, 2,	7.0710−01,	4, 4,	7.0710−01,	4, 8,	−7.0500−01
4,10,	4.4350−01,	4,12,	1.1400+00,	4,14,	1.5810+00	4,16,	1.5563+00
5, 2,	−7.0710−01,	5, 4,	7.0710−01,	5, 8,	−4.9000−01,	5,10,	−5.4040−01
5,12	−1.0500+00	5,14,	1.2600+00,	5,16,	−1.2400+00,	6, 2,	7.0710−01
6, 4,	7.0710−01,	6, 8,	−5.6100−02,	6,10,	2.3600+00,	6,12,	3.6000−01
6,14,	−2.5100+00,	6,16,	−2.0014+00				

Table 6 16-state HAC controller

C Matrix is 4 × 16 (controller gains)							
1, 7,	−8.0143+00,	1, 8,	3.1746+02,	1, 9,	−3.0186+00,	1,10,	2.9813+02
1,11,	−2.2741+01,	1,12,	2.1335+03,	1,15,	7.0675−01,	1,16,	−6.1011+02
2, 1,	2.2580+01,	2, 2,	2.3043+02,	2, 3,	4.2301−02,	2, 4,	1.2149+00
2, 5,	−8.0580+00,	2, 6,	−5.4139+00,	2, 7,	9.5711−01	2, 8,	−6.8076+00
2, 9,	−3.2153+01,	2,10,	1.1389+03,	2,11,	−1.0589+01,	2,12,	6.0269+02
2,13,	−1.8406−01,	2,14,	−1.3200+02,	2,15	−3.7400+00,	2,16,	1.4535+03
3, 1,	−1.9161+01,	3, 2,	−2.0442+02,	3, 3,	−3.5128+01,	3, 4,	−3.8688+02
3, 5,	−4.9838+00,	3, 6,	−3.6438+00,	3, 7,	1.2846+01,	3, 8,	−1.6907+02
3, 9,	2.8698+00,	3,10,	4.1339+02,	3,11,	−2.0727+01,	3,12,	2.5775+03
3,13,	−5.9945+00,	3,14,	1.4256+03,	3,15,	−2.4859+00,	3,16,	1.0485+03
4, 1,	−1.9292+01,	4, 2,	−2.0585+02	4, 3,	3.4959+01,	4, 4,	3.8600+02
4, 6,	−3.7899+00,	4, 7,	−1.1272+01,	4, 8,	2.0386+02,	4, 9,	3.3141+00
4,10,	3.6721+02,	4,11,	−2.1264+01,	4,12,	1.8654+03,	4,13,	5.6083+00
4,14,	−1.6902+03,	4,15,	−2.4749+00,	4,16,	1.0184+03,		
K Matrix is 16 × 6 (filter gains)							
1, 1,	−5.4020−01,	1, 2,	3.0760−02,	1, 3,	−5.0296−01,	1, 4,	5.0935−01
1, 5,	−5.2185−01,	1, 6,	4.8587−01,	2, 1,	−4.8365−02,	2, 2,	5.7741−03
2, 3,	−4.9480−02,	2, 4,	5.0145−02,	2, 5,	−5.0875−02,	2, 6,	4.8257−02
3, 1,	−8.0557−03,	3, 2,	4.4646−03,	3, 3,	6.5006−01,	3, 4,	5.3580−01
3, 5,	5.8599−01,	3, 6,	6.4061−01,	4, 1,	−8.0697−04,	4, 2,	4.6836−04
4, 3,	6.4048−02,	4, 4,	5.4350−02,	4, 5,	5.8701−02,	4, 6,	6.3399−02
5, 1,	1.8188−02,	5, 2,	2.1916−02,	5, 3,	−3.1850−03,	5, 4,	3.4430−03
5, 5,	−3.4781−03,	5, 6,	3.0506−03,	6, 1,	1.1680−02,	6, 2,	1.4316−02
6, 3,	−2.3486−03,	6, 4,	2.4914−03,	6, 5,	−2.5053−03,	6, 6,	2.2712−03
7, 1,	1.1203−01,	7, 2,	9.4937−02,	7, 3,	−4.2036−02,	7, 4,	1.5184+01
7, 5,	1.0757+01,	7, 6,	−5.6227−01,	8, 1,	3.7197−03,	8, 2,	−4.5848−03
8, 3,	−2.3674−02,	8, 4,	−1.1699−01,	8, 5,	−9.8171−02,	8, 6,	−2.3207−02
9, 1,	−1.9204+00,	9, 2,	1.7580−01,	9, 3,	3.1287+00,	9, 4,	−3.0911−01
9, 5,	5.3617−01,	9, 6,	−3.8630+00,	10, 1,	8.2535−03,	10, 2,	1.9964−03
10, 3,	−1.9745−02,	10, 4,	2.1622−03,	10, 5	−2.5164−03,	10, 6,	2.3384−02
11, 1,	−2.7771+00,	11, 2,	6.7458+00,	11, 3,	1.2731+00,	11, 4,	−1.2492+01
11, 5,	1.3033+01,	11, 6,	−1.9679+00,	12, 1,	2.3230−03,	12, 2,	−8.1305−03
12, 3,	−1.5041−02,	12, 4,	2.3977−02,	12, 5,	−1.7514−02,	12, 6,	1.8949−02
13, 1,	1.0374−01,	13, 2,	4.0077−03,	13, 3,	4.7717+00,	13, 4,	−2.8962+00
13, 5,	−2.6341+00,	13, 6,	4.8204+00,	14, 1,	−3.4239−04,	14, 2,	−5.6593−06
14, 3,	8.5517−03,	14, 4,	−5.2532−03,	14, 5,	−4.0111−03,	14, 6,	9.9023−03
15, 1,	−1.9225+00,	15, 2,	−3.2375−02,	15, 3,	−4.3681+00,	15, 4,	−2.7782+00
15, 5,	2.4529+00,	15, 6,	4.9200+00,	16, 1,	−5.4845−03,	16, 2,	−4.5929−04
16, 3,	−1.1506−02,	16, 4,	−6.5950−03,	16, 5,	7.2200−03,	16, 6,	1.1133−02

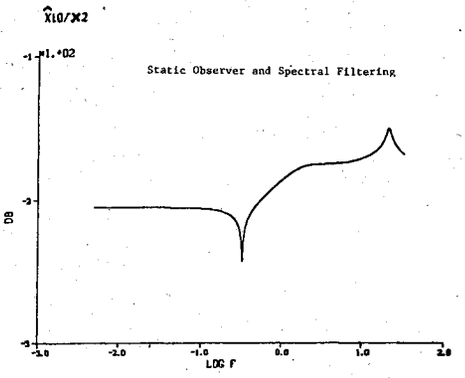

Fig. 12 Modified static observer rejection of irrelevant modes.

accuracy of the matrices G and H. Direct measurements were performed using sine-wave excitations at the various modal frequencies and the model was updated. The final model, which included the three rigid body and the first five bending modes, is shown in Table 5, where the matrices F and G have been converted to their discrete equivalents Φ and Γ.

The 16-States HAC Control Experiment

From the model described above, a full 16th-order controller was designed. The gain matrices C and K, corresponding to the controller and the filter, respectively, are given in Table 6. These gains were loaded in the AP with the coefficient matrices Φ, Γ, and H. The control actuators were the left PPM actuator and the three CEM actuators. No anti-aliasing filtering was performed on the sensor signal because of unacceptable phase rotations that this filtering produces. However, a mild second-order filter was used on the control inputs to avoid excessive roughness in the actuator output forces which otherwise would tend to excite a wide spectrum of higher frequency modes.

The closed-loop tests were conducted by exciting actuator 5 (PPM) with a chirp (fast frequency sweep) between 1 and 60 Hz.

The system was stable and the time histories of the various responses are shown in Figs. 13-16. This series of charts shows the characteristics of a successful controller for the plate that acts on three rigid body modes and the five lowest bending modes (18.1, 19.1, 26.2, 40, and 43.4 Hz). Figure 13 shows the four actuator responses to a wide-band chirp excitation by one proof-mass actuator (PPM). Control activity appears as the excitation frequency sweeps through plate resonances. Most of the activity is in the first five modes, where the controller increases damping significantly. The PPM actuator participates significantly in controlling the bending modes.

The time histories of the excitation and the six sensor signals used by the optimal filter are shown next in Fig. 14. Modal excitations are seen occurring at different times in different channels as the input frequency sweeps through the various resonances of the plate. The varied modal response

among the sensors reflects the various observability of each mode by each sensor.

The traces of Fig. 15 are those of the complete sensor system, six for control plus two for independent checking and characterization. Since the rigid body translation was only lightly controlled, the displacement sensors (1, 2, 7, and 8) show more low-frequency activity than the other sensors. Finally, the static observer output is shown in Fig. 16. Higher frequency modes, not modeled by this observer, corrupt these modal responses. Thus, a Kalman filter is absolutely necessary in this case, where the number of modes to be controlled exceeds the number of sensors, to estimate all the bending modes to be controlled properly.

From the previous data, more specific information may be obtained by further processing. For instance, transfer functions, such as the one shown in Fig. 17 where phase and amplitude are displayed, give a quick estimation of resonances and damping.

Quantitative values can be obtained by curve-fitting techniques. Figure 18 shows an example of such methods. In the case shown, a function of the form

$$T(\omega) = \sum_{1}^{4} \frac{A_n + jB_n}{\omega_n^2 - \omega^2 + 2j\zeta_n\omega_n}$$

(represented by the continuous lines) was fitted to the measured transfer function (dotted line) by adjusting the parameters A_n, B_n, ω_n, and ζ_n. Sensor 5 was close to a nodal line for the 19.75 Hz mode; thus, no response could be observed at that frequency for this particular sensor. Therefore, data from other sensors was needed to identify the 19.75 Hz mode as shown in Fig. 19. The above identification of modal frequencies and dampings was performed using the Vibration Analysis and Measurement Processor (VAMP) program. The results of the closed-loop identification of the previous figures are summarized in Table 7 showing an excellent agreement with the predicted frequencies and dampings. The purely open-loop results are not shown because they differ only slightly in frequency from the LAC case. The damping ratios, however, were quite different, one to two orders of magnitude lower. Where the LAC brings only approximately 1% damping, the HAC system achieves more than 10% as predicted. The doubling up in the predicted frequencies is due to the addition of the filter roots (denoted by f) to the controller roots (denoted by c). While the uncontrolled structure was of order 16, the closed-loop system becomes truly a 32nd-order system, and mode shapes can be significantly affected by this coupling with the filter. The damping ratios were subsequently re-evaluated using the more precise maximum likelihood (ML) method. They are listed in the table and turned out to be lower than those obtained with VAMP. This difficulty of estimating damping ratios larger than 10% is typical of the identification problem of closed-loop structures.

A final overview of the effect of the control system is shown in Fig. 20, where the open-loop and closed-loop response of

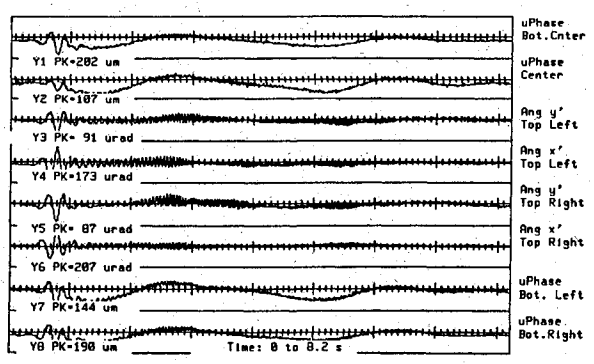

Fig. 15 Time histories of control sensors and evaluation sensors output.

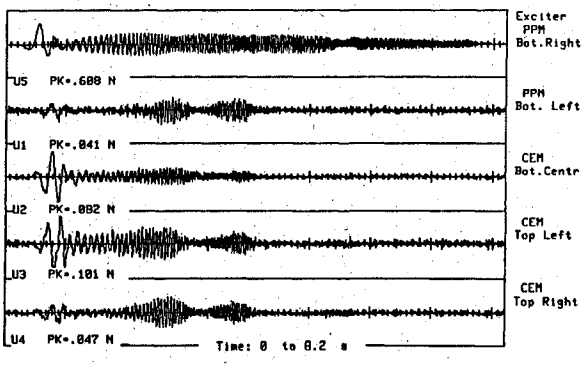

Fig. 13 Time histories of excitation force and control inputs.

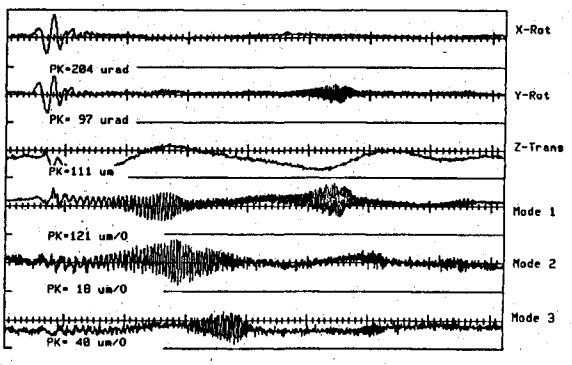

Fig. 16 Time histories of static observer output.

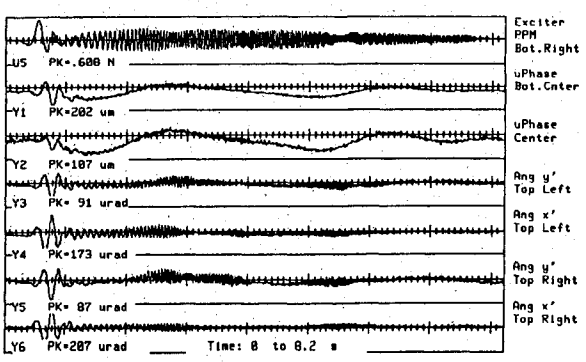

Fig. 14 Time histories of excitation force and sensor outputs.

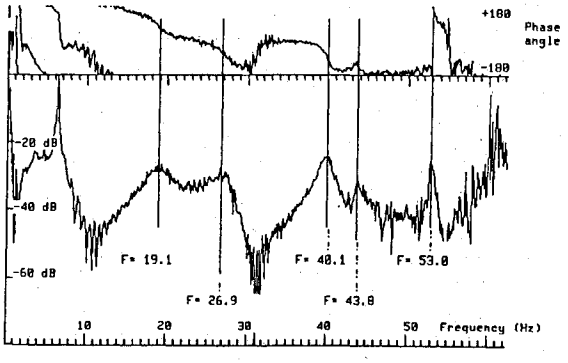

Fig. 17 Closed-loop transfer function from excitation to sensor 5.

Table 7 Results of closed-loop identification

Closed-loop poles								
			HAC and LAC					
LAC only			Predicted		Measured		Max. likelihood	
Frequency	Damping		Frequency	Damping	Frequency	Damping	Frequency	Damping
0.194	0.005	c[a]	0.55	0.22	–	–		
		f[b]	0.64	0.41				
0.324	0.005	c	2.52	0.70				
		f	2.52	0.71	–	–		
0.519	0.005	c	2.68	0.70				
		f	2.62	0.70	–	–		
18.15	0.018	c	18.60	0.15				
		f	18.30	0.15	18.48	0.15	18.7	0.095
19.07	0.009	c	19.57	0.15				
		f	19.18	0.12	19.75	0.15	19.94	0.071
26.62	0.008	c	26.95	0.10	26.96	0.09	26.95	0.036
		f	26.63	0.10	26.61	0.11	26.66	0.048
39.50	0.010	c	39.59	0.04	39.67	0.03	39.73	0.019
		f	39.51	0.05	39.56	0.03	39.62	0.021
		c	43.43	0.02			43.78	0.022
43.40	0.001	f	43.42	0.04	43.73	0.03	43.89	0.040

[a] c = controller, [b] f = filter.

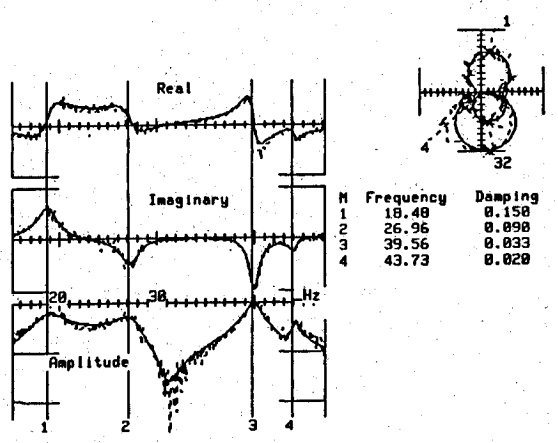

Fig. 18 Modal identification of Y5 sensor data using curve fitting technique (VAMP).

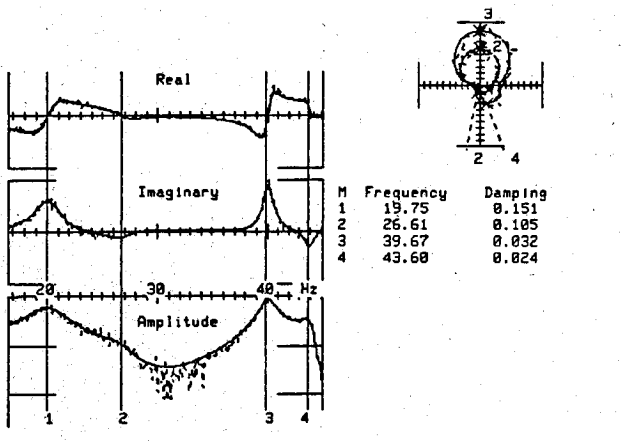

Fig. 19 Modal identification of Y6 sensor data using curve fitting technique (VAMP).

the plate is described by the response of the combined output from sensors 5 and 6. This combination was used so that both modes at 18 and 19 Hz could be seen at once. This result was obtained using a spectrum analysis and a slow sine sweep of the exciter. The rigid body (low-frequency side) is not behaving as expected, showing low damping characteristics. However, the frequency has been pushed up to about 3 Hz as predicted. This rigid body behavior seems to be a recurring problem and was observed in other experiments as well. It is not clear at this time what sort of model error contributes to it.

Further Remarks on Modeling

From the diagrams of Fig. 5, one can see definite symmetry patterns in the various mode shapes and may be tempted to take advantage of these symmetries to obtain decoupled sets of equations. The "rigid body modes" (not shown), consisting mainly of yaw, pitch, and piston motions are decoupled by virtue of their definition, i.e., they actually represent the motion of an idealized frame, or undeformed structure, about which structural deformations take place in an infinitesimal sense. In general, mode shapes can be separated into two categories: the symmetric and antisymmetric (with respect to the Y axis) modes. By choosing an actuator set with similar properties, separation theoretically can be obtained between symmetric and antisymmetric model dynamics. However, Fig. 5 is valid only for a perfect, unrestrained circular plate. In the physical model, this symmetry breaks down because the suspension system is not attached to the center of mass and the actuator locations and masses are not distributed with the same symmetry. Although such decoupling might have provided a sufficiently accurate model (as was the case in a previous experiment, TOYSAT,[3]) this option was not exercised here because it was felt that it lacked generality, and the purpose of the plate experiment was to be generic.

The actuator locations were nonetheless chosen to provide the best controllability for the first few modes. On returning to Fig. 5, it can be seen by comparison with Fig. 4 that there are always some actuators where some modal activity is present, at least for the 11 modes shown. The same is true for the sensors. A more quantitative view of these observability and controllability questions can be gained from the examination of the G and H matrices of Table 5, where the effect of each actuator on each modal state and that of each modal state on each sensor is represented by the corresponding matrix element, respectively.

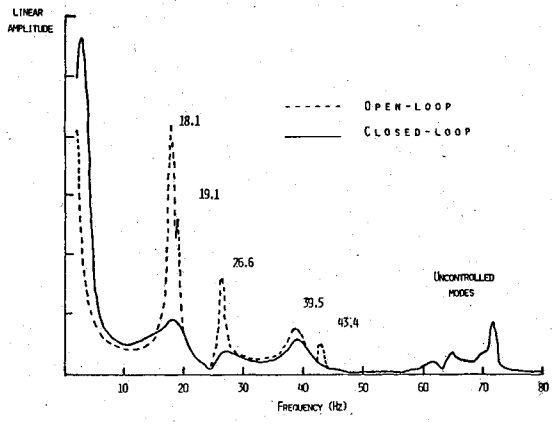

Fig. 20 Combined open-loop and closed-loop frequency responses of sensors 5 and 6.

Finally a word should be said about the accuracy of the control model. The closed-loop results shown in Table 7 indicate good agreement between predicted and measured behavior of the system. From a purely pragmatic point of view, one may thus be satisfied with the accuracy of the control model. However, more system identification would be needed to establish the accuracy or inaccuracy of this model in itself. In fact, is is almost certain to be different from the physical model, since it is a finite-order model in which the effect of the unmodeled (truncated) modes has been minimized by the control law itself (gain stabilization due to limited bandwidth, LAC interaction, etc.). It is thus a significant question which is now receiving more attention in the context of system identification theories and experimental verifications.

Significant Results of the Plate Experiment

Table 8 describes the most significant results and achievements of the plate experiment. The main and most significant achievement of the ACOSS program is that it created the possibility of closing the loop on a very lightly damped two-dimensional structure with a relatively high-order (16th) optimal controller and obtained significant amounts of damping (up to 10%) as theoretically predicted. Because the rigid body modes were part of the controlled variables and because of the high performance characteristics of this system (10 μrad accuracy range), this experiment puts the program one step further toward real space applications. Also, the use of newly developed actuators and sensors is quite significant.

Table 8 Circular plate experiment significant results

Experimental validation of ACOSS technology achieved in the following areas:
HAC/LAC control methodology verified
Significant amounts of modal damping obtained
Proof-mass actuators used in HAC schemes
Multichannel μ- phase sensor applied to structural control
Digital implementation demonstrated on high-order system

Conclusions

These experiments have been very successful in achieving their purpose of validating the control methodology. They also indicated that improvement in system performance will require progress in the areas of system identification and modeling, filter design, rigid body interactions, digital mechanizations, and actuator/sensor accuracy.

From the experimental results, it is seen that performance limitations and problems require more attention in the areas mentioned above. Performance is strongly related to model accuracy, thus identification is of prime importance. Filter design is also an uncertain area because of its dependence upon model errors; more theory is needed. The rigid body effects are not as yet well understood and have been noticed both in the laboratory and in simulations. Finally, better architecture is needed for microprocessor implementation of fast, high-order, control algorithms.

References

[1] Strunce, R. et al., "An Investigation of Enabling Technologies for Large Precision Space Systems," Charles Stark Draper Laboratory CSDL-R-1499, Vol. III, Nov. 1981.

[2] "ACOSS 12 Final Report," Lockheed Missiles and Space Co., for DARPA, LMSC D833023, July 1983.

[3] "ACOSS Five, Phase 1A, Final Technical Report," Rome Air Defense Center RADC-TR-82-21, March 1982.

[4] "ACOSS 12 Interim Report," Lockheed Missiles and Space Company for DARPA, Sept. 1982.